ELSEVIER

Journal of Molecular Structure (Theochem) 501–502 (2000) 353–367

THEO CHEM

www.elsevier.nl/locate/theochem

Molecular excitation energies from time-dependent density functional theory ☆

T. Grabo, M. Petersilka, E.K.U. Gross*

Institut für Theoretische Physik, Universität Würzburg, Am Hubland, 97074 Würzburg, Germany

Abstract

The performance of various exchange-correlation functionals is evaluated in the calculation of molecular excitation energies from time-dependent density functional theory. Excitation energies of N_2 and CO are reported, using either the local density approximation (LDA) for exchange and correlation or an orbital functional in the approximation of Krieger, Li and Iafrate. The latter is based on exact exchange plus a correlation contribution in the form suggested by Colle and Salvetti. While the LDA proves to work remarkably well for the lower excited states due to error cancellations, self-interaction-free potentials are essential for a good description of higher lying states. © 2000 Elsevier Science B.V. All rights reserved.

Keywords: Molecular excitation energies; Time-dependent density functional theory; Local density approximation

1. Introduction and dedication

It is a great pleasure for us to contribute to this scientific celebration of Professor Rezso Gáspár. With his suggestion of a local exchange potential, Gáspár was among the pioneers of a theory which, since the work of Hohenberg, Kohn and Sham [1,2], has been termed density-functional theory (DFT). Over the years, the available approximations for the local exchange potential have steadily improved [3–5]. The *variationally best* local exchange potential is obtained if the Hartree–Fock total energy is varied under the subsidiary condition that the orbitals come from a local potential. The resulting so-called *optimized effective potential*, when complemented with a suitable correlation contribution, was recently shown to yield atomic ground-state properties in close agreement with results based on configuration interaction calculations [6]. In the present paper, we will investigate the performance or this optimized effective potential in the calculation of molecular excitation energies.

As far as the determination of excitation spectra is concerned, several extensions of ground-state DFT have been proposed. They are based either on the Rayleigh–Ritz principle for the lowest eigenstate of a given symmetry class [7–9] or on a variational principle for ensembles [10–23]. A major difficulty lies in the fact that the exchange-correlation (xc) functionals associated with these approaches are not identical with the ordinary ground-state xc energy functional, although the latter sometimes gives rather accurate results [23]. In principle, the xc functional in these approaches should depend either on the symmetry labels of the prescribed symmetry class or on the particular ensemble considered, and very little is known about the nature of this dependence. To circumvent this problem, we recently proposed [24–28] a different approach for the calculation of excitation energies, which is based on time-dependent

☆ Dedicated to Professor R. Gáspár on the occasion of his 80th year.

* Corresponding author.

PII: S0166-1280(99)00445-5

density-functional theory (TDDFT) [29]. This method makes use of the fact that excitation energies may be obtained from the poles of the linear density response function which can be expressed, in principle exactly, in terms of the response function of a noninteracting Kohn–Sham (KS) system and a frequency-dependent exchange-correlation kernel. In this way, corrections to the KS orbital energy differences (which are the poles of the KS response function) are obtained, which shift them towards the true excitation energies of the fully interacting system. As input, the resulting computational scheme only requires *ground state* properties, i.e. occupied and virtual orbitals of the KS potential corresponding to the *ground-state* of a given physical system. Recent applications to atoms [27,28,30–32], molecules [33–38] and clusters [39–41] are highly promising. In particular, the successful calculation of the excited-state potential energy surfaces of formaldehyde [38] has shown that TDDFT is also capable of describing the strong mixing with Rydberg transitions and the corresponding avoided crossings. In view of these successes, one can expect that this scheme will become a standard method for the calculation of excitation energies of finite many-particle systems.

The accuracy of any density functional method, however, crucially depends on the quality of the functional approximations involved. The purpose of this work is to investigate the role of the static KS potential from which the orbitals and orbital energies entering the scheme are calculated. Furthermore, we address the influence of the necessary truncation of the matrix equation from which the corrections to the KS orbital energy differences have to be determined.

This article is organized as follows: In Section 2, a brief review of the underlying theory is given. In Section 3, the employed approximate functionals are described. Section 4 discusses the numerical results obtained for diatomic molecules, followed by a summary in Section 5.

2. Basic formalism

The calculation of excitation energies from time-dependent DFT makes use of the fact that the full linear density response $\rho_{1\sigma}$ of a system of interacting electrons with spin σ subject to a frequency-dependent perturbation $V_{1\sigma'}(\mathbf{r}', \omega)$ has poles at the exact excitation energies (see Ref. [42]). In terms of the density–density response function $\chi_{\sigma,\sigma'}$ of interacting electrons, the frequency-dependent density response $\rho_{1\sigma}(\mathbf{r},\omega)$ is given by

$$\rho_{1\sigma}(\mathbf{r}, \omega) = \sum_{\sigma'} \int \mathrm{d}^3 r' \chi_{\sigma,\sigma'}(\mathbf{r}, \mathbf{r}', \omega) V_{1\sigma'}(\mathbf{r}', \omega). \tag{1}$$

Alternatively, the time-dependent generalization of DFT allows one to express the exact density response $\rho_{1\sigma}$ via the response function $\chi_{s\sigma,\sigma'}$ of the noninteracting KS system [27]:

$$\rho_{1\sigma}(\mathbf{r}, \omega) = \sum_{\sigma'} \int \mathrm{d}^3 r' \chi_{s\sigma\sigma'}(\mathbf{r}, \mathbf{r}', \omega) V_{s1\sigma'}(\mathbf{r}', \omega). \tag{2}$$

In the above equation, $V_{s1\sigma'}$ is the linearized time-dependent KS potential given by

$$V_{s1\sigma'}(\mathbf{r}', \omega) = V_{1\sigma'}(\mathbf{r}', \omega) + \sum_{\sigma''} \int \mathrm{d}^3 r'' \left(\frac{1}{|\mathbf{r}' - \mathbf{r}''|} + f_{\mathrm{xc}\sigma'\sigma''}(\mathbf{r}', \mathbf{r}'', \omega) \right) \times \rho_{1\sigma''}(\mathbf{r}'', \omega). \tag{3}$$

The spin-dependent xc kernel f_{xc} is defined as the Fourier transform of

$$f_{\mathrm{xc}\sigma\sigma'}(\mathbf{r}, t, \mathbf{r}', t') := \left. \frac{\delta V_{\mathrm{xc}\sigma}[\rho_\uparrow, \rho_\downarrow](\mathbf{r}, t)}{\delta \rho_{\sigma'}(\mathbf{r}', t')} \right|_{\rho_{\mathrm{GS}_\uparrow}, \rho_{\mathrm{GS}_\downarrow}} \tag{4}$$

evaluated at the ground-state spin densities $\rho_{\mathrm{GS}_\uparrow}$, $\rho_{\mathrm{GS}_\downarrow}$ of the unperturbed system. The response function of the KS system can be expressed in terms of the stationary KS-orbitals

$$\chi_{s\sigma\sigma'}(\mathbf{r}, \mathbf{r}', \omega) = \delta_{\sigma\sigma'} \sum_{j,k} (f_{k\sigma} - f_{j\sigma}) \frac{\varphi_{j\sigma}(\mathbf{r}) \varphi^*_{k\sigma}(\mathbf{r}) \varphi^*_{j\sigma}(\mathbf{r}') \varphi_{k\sigma}(\mathbf{r}')}{\omega - (\epsilon_{j\sigma} - \epsilon_{k\sigma}) + i\eta}, \tag{5}$$

where $f_{i\sigma}$ denote the Fermi-occupation factors (1 or 0).

With these definitions, Eq. (2) may be rewritten as

an integral equation for the linear density response:

$$\sum_{\sigma''}\int \mathrm{d}^3r''\Bigg[\delta_{\sigma\sigma''}\delta(\mathbf{r}-\mathbf{r}'') - \sum_{\sigma'}\int \mathrm{d}^3r'\chi_{s\sigma\sigma'}(\mathbf{r},\mathbf{r}';\omega) \times\left(\frac{1}{|\mathbf{r}'-\mathbf{r}''|}+f_{\mathrm{xc}\sigma'\sigma''}(\mathbf{r}',\mathbf{r}'';\omega)\right)\Bigg]\rho_{1\sigma''}(\mathbf{r}'',\omega) = \sum_{\sigma'}\int \mathrm{d}^3r'\chi_{s\sigma\sigma'}(\mathbf{r},\mathbf{r}';\omega)V_{1\sigma'}(\mathbf{r}',\omega). \tag{6}$$

In general, the true excitation energies Ω are not identical with the Kohn–Sham excitation energies $\epsilon_{j\sigma}-\epsilon_{k\sigma}$. Therefore, the right-hand side of Eq. (6) remains finite for $\omega\rightarrow\Omega$.. Since, on the other hand, the exact spin-density response $\rho_{1\sigma}$, has poles at the true excitation energies Ω, the integral operator acting on $\rho_{1\sigma}$ on the left-hand side of Eq. (6) cannot be invertible for $\omega\rightarrow\Omega$. (Assuming the existence of the inverse operator, its action on both sides of Eq. (6) results in a finite right-hand side for $\omega\rightarrow\Omega$. This leads to a contradiction since $\rho_{1\sigma}$, remaining on the left-hand side, has a pole at $\omega=\Omega$.)

Consequently, the true excitation energies Ω are characterized as those frequencies where the eigenvalues of the integral operator acting on the spin-density vector in Eq. (6) vanish. Integrating out the delta-function in Eq. (6), the true excitation energies Ω are those frequencies, where the eigenvalues $\lambda(\omega)$ of

$$\sum_{\sigma'}\int \mathrm{d}^3r'\chi_{s\sigma\sigma'}(\mathbf{r},\mathbf{r}';\omega)\sum_{\sigma''}\int \mathrm{d}^3r'' \times\left(\frac{1}{|\mathbf{r}'-\mathbf{r}''|}+f_{\mathrm{xc}\sigma'\sigma''}(\mathbf{r}',\mathbf{r}'';\omega)\right)\gamma_{\sigma''}(\mathbf{r}'',\omega) = \lambda(\omega)\gamma_{\sigma}(\mathbf{r},\omega) \tag{7}$$

satisfy

$$\lambda(\Omega)=1. \tag{8}$$

This condition rigorously determines the true excitation spectrum of the interacting system at hand.

For a single-particle transition ($k\rightarrow j$) we introduce the notation

$$q\equiv(j,k). \tag{9}$$

The corresponding transition energies are

$$\omega_{q\sigma}=\epsilon_{j\sigma}-\epsilon_{k\sigma}. \tag{10}$$

Moreover, we define

$$\Phi_{q\sigma}(\mathbf{r}):=\phi_{k\sigma}(\mathbf{r})^*\phi_{j\sigma}(\mathbf{r}), \tag{11}$$

$$\alpha_{q\sigma}:=f_{k\sigma}-f_{j\sigma}, \tag{12}$$

and set

$$\xi_{q\sigma}(\omega):=\sum_{\sigma''}\int \mathrm{d}^3r'\int \mathrm{d}^3r''\Phi_{q\sigma}(\mathbf{r}')^* \times\left(\frac{1}{|\mathbf{r}'-\mathbf{r}''|}+f_{\mathrm{xc}\sigma\sigma''}(\mathbf{r}',\mathbf{r}'';\omega)\right)\gamma_{\sigma''}(\mathbf{r}'',\omega). \tag{13}$$

Using these definitions, Eq. (7) can be recast into

$$\sum_{q}\frac{\alpha_{q\sigma}\Phi_{q\sigma}(\mathbf{r})}{\omega-\omega_{q\sigma}+\mathrm{i}\eta}\xi_{q\sigma}(\omega)=\lambda(\omega)\gamma_{\sigma}(\mathbf{r},\omega). \tag{14}$$

Solving this equation for $\gamma_\sigma(\mathbf{r},\omega)$ and reinserting the result on the right-hand side of Eq. (13) we arrive at

$$\sum_{\sigma'}\sum_{q'}\frac{M_{q\sigma q'\sigma'}(\omega)}{\omega-\omega_{q'\sigma'}+i\eta}\xi_{q'\sigma'}(\omega)=\lambda(\omega)\xi_{q\sigma}(\omega), \tag{15}$$

where we have introduced the matrix elements

$$M_{q\sigma q'\sigma'}(\omega)=\alpha_{q'\sigma'}\int \mathrm{d}^3r\int \mathrm{d}^3r'\ \Phi^*_{q\sigma}(\mathbf{r}) \times\left(\frac{1}{|\mathbf{r}-\mathbf{r}'|}+f_{\mathrm{xc}\sigma\sigma'}(\mathbf{r},\mathbf{r}';\omega)\right)\Phi_{q'\sigma'}(\mathbf{r}'). \tag{16}$$

Introducing the quantity $\beta_{q\sigma}:=\xi_{q\sigma}(\Omega)/(\Omega-\omega_{q\sigma})$ and using the condition (8), we can, at the correlated excitation energies $\omega=\Omega$, rewrite Eq. (15) in the following form:

$$\sum_{\sigma'}\sum_{q'}(M_{q\sigma q'\sigma'}(\Omega)+\omega_{q\sigma}\delta_{qq'}\delta_{\sigma\sigma'})\beta_{q'\sigma'}=\Omega\beta_{q\sigma}. \tag{17}$$

Once again, this eigenvalue problem rigorously determines the true excitation spectrum of the interacting system.

In practice, the matrix equation (15) or, alternatively, the eigenvalue problem (17), has to be truncated in one way or another. One possibility consists

in expanding all quantities in Eq. (15) about one particular KS-orbital energy difference[1] $\omega_{p\tau}$. For non-degenerate poles one obtains [27] in lowest order

$$\Omega = \omega_{p\tau} + M_{p\tau p\tau}(\omega_{p\tau}). \tag{18}$$

If the pole $\omega_{p\tau}$ is $\mathscr{P}$-fold degenerate, i.e.

$$\omega_{p_1\tau_1} = \omega_{p_2\tau_2} = \cdots = \omega_{p_{\mathscr{P}}\tau_{\mathscr{P}}} \equiv \omega_0, \tag{19}$$

then, in lowest order, the corresponding excitation energies Ω_n are given by [28]

$$\Omega_n = \omega_0 + \mathrm{Re}\,(A_n(\omega_0)) \tag{20}$$

where the $A_n(\omega_0)$ are the $\mathscr{P}$ eigenvalues of the truncated matrix equation

$$\sum_{k=1}^{\mathscr{P}} M_{p_i\tau_i p_k\tau_k}(\omega_0)\xi^{(n)}_{p_k\tau_k}(\omega_0) = A_n(\omega_0)\xi^{(n)}_{p_i\tau_i}, \qquad i = 1,\ldots,\mathscr{P} \tag{21}$$

This lowest-order result amounts to approximating the KS response function χ_s by the single pole contribution at ω_0 alone. It therefore will be referred to as single-pole approximation (SPA). The resulting excitation energies can be assigned to symmetry labels according to the symmetry of the matrix M in Eq. (21).

Alternatively, Eq. (17) may be truncated by only considering the matrix elements corresponding to a particular single-particle transition ($k \rightarrow j$) *and* the reverse transition ($j \rightarrow k$), denoted by $\mathscr{2}$ and $\bar{\mathscr{2}}$, respectively. This leads to the following eigenvalue problem:

$$\sum_{\sigma'}\sum_{q'=\mathscr{2},\bar{\mathscr{2}}} (M_{q\sigma q'\sigma'}(\Omega) + \omega_{q\sigma}\delta_{qq'}\delta_{\sigma\sigma'})\beta_{q'\sigma'} = \Omega\beta_{q\sigma}. \tag{22}$$

We will refer to this scheme as small matrix approximation (SMA).

In the framework of traditional quantum chemistry, Eq. (17) is usually solved by expanding the orbitals and potentials in a basis set. This has the advantage that a proper choice of the basis can lead to a good representation of the continuum contributions (see, for example Ref. [43]). However, even with very large basis sets stability and convergence problems have been reported [33]. Results from fully numerical codes that solve the KS equations on a grid have the advantage of being free of errors caused by the finite size of the basis set. The disadvantage is that one can consider only bound orbitals, as states with positive energy are not represented accurately.

[1] This is justified if the true excitation energy Ω is not too far from the KS orbital energy difference $\omega_{p\tau}$.

3. Approximate functionals

Apart from the truncation of the matrix equations (15) or (17) described in Section 2, two further approximations are necessary: (i) in the calculation of the KS orbitals $\phi_k(\mathbf{r})$ and their eigenvalues ϵ_k, one employs some approximation of the static xc potential V_{xc}. (ii) The functional form of the dynamic xc kernel f_{xc} needs to be approximated.

In this work, two approximations of the exchange-correlation potential are used: (i) the LDA in the parameterization of Vosko, Wilk and Nusair [44] and (ii) orbital dependent xc functionals

$$E_{xc}[\{\varphi_{i\sigma}\}] = E_x^{\mathrm{exact}}[\{\varphi_{i\sigma}\}] + E_c[\{\varphi_{i\sigma}\}] \tag{23}$$

including the exact exchange energy expression

$$E_x^{\mathrm{exact}}[\{\varphi_{i\sigma}[\rho]\}] = -\frac{1}{2}\sum_{\sigma=\uparrow,\downarrow}\sum_{j,k=1}^{N_\sigma} \times \int \mathrm{d}^3r \int \mathrm{d}^3r' \frac{\varphi^*_{j\sigma}(\mathbf{r})\varphi^*_{k\sigma}(\mathbf{r}')\varphi_{k\sigma}(\mathbf{r})\varphi_{j\sigma}(\mathbf{r}')}{|\mathbf{r}-\mathbf{r}'|}. \tag{24}$$

The corresponding xc potential is evaluated using the semi-analytical method of Krieger, Li and Iafrate (KLI) [45–51] given by

$$V_{xc\sigma}(\mathbf{r}) \approx \frac{1}{\rho_\sigma(\mathbf{r})}\sum_{i=1}^{N_\sigma}|\varphi_{i\sigma}(\mathbf{r})|^2[u_{xci\sigma}(\mathbf{r}) + (\bar{V}^{\mathrm{KLI}}_{xci\sigma} - \bar{u}_{xci\sigma})] \tag{25}$$

with

$$u_{xci\sigma}(\mathbf{r}) := \frac{1}{\varphi^*_{i\sigma}(\mathbf{r})}\frac{\delta E_{xc}[\varphi_{j\sigma}]}{\delta\varphi_{i\sigma}(\mathbf{r})}. \tag{26}$$

The constants $(\bar{V}^{\mathrm{KLI}}_{xci\sigma} - \bar{u}_{xci\sigma})$ denote average values taken over the density of the $i\sigma$ orbital, i.e.

$$\bar{u}_{xci\sigma} = \int \mathrm{d}^3r|\varphi_{i\sigma}(\mathbf{r})|^2 u_{xci\sigma}(\mathbf{r}) \tag{27}$$

Table 1
Orbital energies for N_2 at $R = 2.0744$ a.u. from various DFT approaches

	xcLDA	xcLDA[a]	KLI	KLICS
E_{TOT}	−108.6999	−108.6957	−108.9852	−109.4629
Occupied orbitals				
$1\sigma_g$	−13.9666	−13.9677	−14.3728	−14.4126
$1\sigma_u$	−13.9652	−13.9662	−14.3715	−14.4113
$2\sigma_g$	−1.0379	−1.0411	−1.3061	−1.3384
$2\sigma_u$	−0.4938	−0.4939	−0.7457	−0.7754
$1\pi_u$	−0.4370	−0.4366	−0.6809	−0.7131
$3\sigma_g$	−0.3826	−0.3840	−0.6303	−0.6605
Unoccupied orbitals				
$1\pi_g$	−0.0813	−0.0816	−0.3100	−0.3412
$4\sigma_g$	−0.0015	0.0000	−0.1854	−0.1988
$2\pi_u$	> 0	0.0235	−0.1486	−0.1582
$3\sigma_u$	> 0	0.0114	−0.1300	−0.1390
$1\delta_g$	> 0	–	−0.1016	−0.1081
$5\sigma_g$	> 0	0.0305	−0.0914	−0.0986
$6\sigma_g$	> 0	–	−0.0855	−0.0886
$2\pi_g$	> 0	0.0481	−0.0799	−0.0832
$3\pi_u$	> 0	–	−0.0749	−0.0777

[a] Results obtained with a code using a basis set of 106 contracted Gaussian-type orbitals from Ref. [33].

and likewise for $\bar{V}^{KLI}_{xci\sigma}$. In the following, we refer to this scheme as KLI if the exact exchange energy functional (24) is used with correlation contributions neglected. By KLICS we denote the same method with the inclusion of correlation contributions in the form given by Colle and Salvetti [6,52,53,54].

It is a well-known fact that the LDA xc potential falls off exponentially. Consequently, the LDA valence-orbitals are too weakly bound, with orbital energies being in error by up to 100%. Contrary to the LDA, both the KLI and KLICS potential show the correct $-1/r$ tail for large r [55] (for a recent review article see Ref. [56]). This leads to orbital energies very close to the exact ones [6,49,57].

Finally, the frequency-dependent quantity $f_{xc\sigma\sigma'}$ has to be approximated. In the present work we will restrict ourselves to the use of the adiabatic LDA (ALDA) which can be expressed via the quantities

$$f_{xc}^{ALDA}(\mathbf{r},\mathbf{r}';\omega) = \delta(\mathbf{r}-\mathbf{r}')\frac{\partial^2}{\partial\rho^2}(\rho\epsilon_{xc}^{hom}(\rho))\bigg|_{\rho_{GS}(\mathbf{r})} \quad (28)$$

and

$$G_{xc}^{ALDA}(\mathbf{r},\mathbf{r}';\omega) = \delta(\mathbf{r}-\mathbf{r}')\frac{\alpha_{xc}(\rho)}{\mu_0^2\rho}\bigg|_{\rho_{GS}(\mathbf{r})} \quad (29)$$

Here, $\alpha_{xc}(\rho) = (\partial^2/\partial\zeta^2)\ (\epsilon_{xc}^{hom}(\rho,\zeta))|_{\zeta=0}$ is the exchange-correlation contribution to the spin stiffness of the homogeneous electron gas with relative spin-polarization $\zeta = 0$, and μ_0 denotes the Bohr magneton. In our calculations, the parameterizations of Ref. [44] were used for ϵ_{xc} and α_{xc}. The diagonal elements of the spin dependent exchange-correlation kernel are given by

$$f_{xc\uparrow\uparrow} = f_{xc\downarrow\downarrow} = f_{xc} + \mu_0^2 G_{xc}, \quad (30)$$

and the off-diagonal elements read

$$f_{xc\downarrow\uparrow} = f_{xc\uparrow\downarrow} = f_{xc} - \mu_0^2 G_{xc}. \quad (31)$$

In the adiabatic approximation, the Fourier transforms of the time-dependent kernels have no frequency dependence at all. Their value corresponds to the static ($\omega = 0$) limit of the linear response kernels [58]. The frequency dependence however, still enters the scheme via the pole-structure of the non-interacting response-function χ_s.

It is important to realize that, although the formalism makes use of the time-dependent generalization of DFT, only ground-state properties are required in the actual calculation.

4. Numerical results for molecular systems

For calculations on diatomic molecular systems, we used a fully numerical, basis-set free two-dimensional code [54,57], developed from the Xα program written by Laaksonen, Sundholm and Pyykkö [59–61]. The code solves the one-particle Schrödinger equation for diatomic molecules

$$\left(-\frac{\nabla^2}{2} - \frac{Z_1}{|\mathbf{R}_1-\mathbf{r}|} - \frac{Z_2}{|\mathbf{R}_2-\mathbf{r}|} + V_H(\mathbf{r}) + V_{x\sigma}^{KLI}(\mathbf{r})\right)$$
$$\times\varphi_{j\sigma}(\mathbf{r}) = \epsilon_{j\sigma}\varphi_{j\sigma}(\mathbf{r}), \quad (32)$$

where $\mathbf{R}_i$ denotes the location and Z_i the nuclear charge of the ith nucleus in the molecule. The partial differential equation is solved in prolate spheroidal coordinates on a two-dimensional mesh by a

Table 2
Excitation energies for N_2 from an xcLDA-calculation at $R = 2.0744$ a.u. The LDA was employed for V_{xc} and the ALDA for the xc kernels. $\Delta\omega_{KS}$ denotes the KS orbital energy difference. All numbers in mHartrees

State		$\Delta\omega_{KS}$	SPA	SMA	Full[a]	Full[b]	Exp[c]
a $^1\Pi_g$	$3\sigma_g \rightarrow 1\pi_g$	301.4	344.3	341.6	339.4	334.4	342.1
B $^3\Pi_g$			281.0	280.2	280.1	279.3	295.5
a′ $^1\Sigma_u^-$	$1\pi_u \rightarrow 1\pi_g$	355.8	355.8	355.8	355.8	355.0	364.6
B′ $^3\Sigma_u^-$			355.8	355.8	355.8	355.0	355.4
A $^3\Sigma_u^+$			301.6	296.7	296.7	289.6	284.5
w $^1\Delta_u$			378.3	377.6	377.6	375.6	377.4
W $^3\Delta_u$			328.7	327.6	327.6	324.5	326.3
a″ $^1\Sigma_g^+$	$3\sigma_g \rightarrow 4\sigma_g$	381.1	385.3	385.3	385.3	–	448.3
E $^3\Sigma_g^+$			379.9	379.8	379.8	–	441.0
o $^1\Pi_u$	$2\sigma_u \rightarrow 1\pi_g$	412.5	521.3	509.8	509.8	–	500.9
C $^3\Pi_u$			384.9	383.9	383.7	380.7	411.2
c $^1\Pi_u$	$1\pi_u \rightarrow 4\sigma_g$	435.5	435.4	435.3	435.3	–	474.1
$^3\Pi_u$			434.8	434.8	434.9	–	470.3

[a] Neglecting continuum states.
[b] Basis-set calculation including continuum states from Ref. [33].
[c] From Ref. [43].

relaxation method, while the third variable, the azimuthal angle, is treated analytically. The Hartree potential

$$V_H(\mathbf{r}) = \int d^3r' \frac{\rho(\mathbf{r}')}{|\mathbf{r} - \mathbf{r}'|} \tag{33}$$

and the functions $u_{xi\sigma}(\mathbf{r})$ (cf. Eq. (26)) needed for the calculation of the exchange potential $V_{x\sigma}^{KLI}(\mathbf{r})$ (cf. Eq. (25)) are computed as solutions of a Poisson and Poisson-like equation, respectively. In this step, the same relaxation technique as for the solution of the one-particle Schrödinger equation is employed. A very detailed description of the code is given in Ref. [62].

We have applied our method to the nitrogen and carbon monoxide molecules. Both are well-studied systems for which most of the lower excited states have been observed and measured in detail.

In Table 1, we show the ground-state and orbital energies of N_2 obtained with the LDA, KLI and KLICS potentials. Owing to the wrong behaviour of the LDA potential in the asymptotic region, there are only two bound unoccupied orbitals in this approximation. For the KLI and KLICS approaches, leading to the correct $-1/r$ tail of the xc potential, we show the lowest nine unoccupied orbitals, all of which have negative energies. In the second column, the results from Ref. [33] of an LDA calculation using an expansion of the orbitals and potentials into a large contracted Gaussian-type basis are displayed. Comparison with our numerical results in the first column shows that the basis-set-expansion error is fairly small: the total energy is 4.2 mHartrees too high and the orbital energies show an error of the same magnitude. For the calculation of excitation energies, the orbital-energy *differences* are important. They show an error of about 1 mHartree on average. Furthermore, the unbound orbitals with positive energies show a different energetic order as the corresponding ones from the KLI and KLICS calculations. Again, this indicates the poor quality of the LDA potential in the asymptotic region. In addition, this fact is also responsible for the poor quality of the value for ϵ_{HOMO}, which should be equal to the first ionization potential in exact DFT. In LDA, $\epsilon_{HOMO} = -383$ mHartrees, whereas the experimental ionization potential is -573 mHartrees [33]. The KLI value for ϵ_{HOMO} is -630 mHartrees and thus significantly closer to the exact one. However, adding the correlation contribution of Colle and Salvetti to the KLI scheme results in a value which is further away from the exact one than the one obtained within the KLI approach. This indicates that the CS correlation potential needs some improvement when calculating molecular properties.

Table 3
Excitation energies for N_2 from a KLI-calculation at $R = 2.0744$ a.u. The exact exchange functional was employed for V_{xc} in KLI-approximation and the ALDA for the xc kernals. $\Delta\omega_{KS}$ denotes the KS orbital energy difference. All numbers in mHartrees

State		$\Delta\omega_{KS}$	SPA	SMA	Full[a]	Exp[b]
$a\ ^1\Pi_g$	$3\sigma_g \rightarrow 1\pi_g$	320.2	364.1	361.4	358.7	342.1
$B\ ^3\Pi_g$			299.6	298.9	298.7	295.5
$a'\ ^1\Sigma_u^-$	$1\pi_u \rightarrow 1\pi_g$	370.9	370.9	370.9	370.9	364.6
$B'\ ^3\Sigma_u^-$			370.9	370.9	370.9	355.4
$A\ ^3\Sigma_u^+$			317.9	313.4	312.8	284.5
$w\ ^1\Delta_u$			392.7	392.1	392.0	377.4
$W\ ^3\Delta_u$			344.4	343.4	343.2	326.3
$o\ ^1\Pi_u$	$2\sigma_u \rightarrow 1\pi_g$	435.7	545.3	534.2	526.2	500.9
$C\ ^3\Pi_u$			407.7	406.8	406.4	411.2
$a''\ ^1\Sigma_g^+$	$3\sigma_g \rightarrow 4\sigma_g$	444.8	461.5	461.2	458.1	448.3
$E\ ^3\Sigma_g^+$			440.0	440.0	439.7	441.0
$c\ ^1\Pi_u$	$3\sigma_g \rightarrow 2\pi_u$	481.6	480.5	480.5	480.3	474.1
$^3\Pi_u$			479.9	479.9	479.6	470.3
$b\ ^1\Pi_u$	$1\pi_u \rightarrow 4\sigma_g$	495.5	496.1	496.1	496.1	486.6
$^3\Pi_u$			491.8	491.8	492.1	497.8
$c'\ ^1\Sigma_u^+$	$3\sigma_g \rightarrow 4\sigma_u$	500.3	500.8	500.8	498.8	477.0
$^3\Sigma_u^+$			496.9	496.9	496.8	466.9

[a] Using all occupied and the lowest 9 unoccupied orbitals.
[b] From Ref. [43].

Table 4
Excitation energies for N_2 from a KLI-calculation at $R = 2.0744$ a.u. The CS approximation for correlation added to the exact exchange was employed for V_{xc} in KLI-approximation and the ALDA for the xc kernals. $\Delta\omega_{KS}$ denotes the KS orbital energy difference. All numbers in mHartrees

State		$\Delta\omega_{KS}$	SPA	SMA	Full[a]	Exp[b]
$a\ ^1\Pi_g$	$3\sigma_g \rightarrow 1\pi_g$	319.3	363.6	360.9	358.1	342.1
$B\ ^3\Pi_g$			298.5	297.7	297.6	295.5
$a'\ ^1\Sigma_u^-$	$1\pi_u \rightarrow 1\pi_g$	371.9	371.9	371.9	371.9	364.6
$B'\ ^3\Sigma_u^-$			371.9	371.9	371.9	355.4
$A\ ^3\Sigma_u^+$			318.2	313.6	312.9	284.5
$w\ ^1\Delta_u$			394.2	393.5	393.4	377.4
$W\ ^3\Delta_u$			345.1	344.0	343.8	326.3
$o\ ^1\Pi_u$	$2\sigma_u \rightarrow 1\pi_g$	434.2	544.8	533.5	525.9	500.9
$C\ ^3\Pi_u$			406.0	405.0	404.7	411.2
$a''\ ^1\Sigma_g^+$	$3\sigma_g \rightarrow 4\sigma_g$	461.7	479.8	479.5	476.3	448.3
$E\ ^3\Sigma_g^+$			456.4	456.3	456.1	441.0
$c\ ^1\Pi_u$	$3\sigma_g \rightarrow 2\pi_u$	502.3	501.3	501.3	500.8	474.1
$^3\Pi_u$			500.3	500.3	499.9	470.3
$b\ ^1\Pi_u$	$1\pi_u \rightarrow 4\sigma_g$	514.3	515.3	515.3	515.3	486.6
$^3\Pi_u$			510.2	510.2	510.6	497.8
$c'\ ^1\Sigma_u^+$	$3\sigma_g \rightarrow 3\sigma_u$	521.5	522.4	522.4	519.9	477.0
$^3\Sigma_u^+$			517.6	517.6	517.4	466.9

[a] Using all occupied and the lowest 9 unoccupied orbitals.
[b] From [43].

In Table 2 results are given for the vertical excitation energies of N_2, calculated from the LDA xc-potential. Apart from the molecular state, the orbital transition and the orbital-energy difference, the excitation energies are shown for different truncations of the exact matrix equation (15) as discussed in Section 3. With our numerical code, we have taken into account all occupied states for the solution of the "full" matrix Eq. (17). For comparison, we also show results which include continuum contributions from a calculation using the same basis set as the one used for the results shown in Table 1, taken from Ref. [33]. The method used in these calculations is identical to the one outlined in Section 3. Finally, the last column displays experimental values taken from [43]. It is evident from the table, that the SPA (Eq. (21)) gives results in good agreement with the ones from the solution of the full matrix equation. The deviation is a few mHartrees, being largest for the $o\ ^1\pi_u$ state with 11.5 mHartrees. As the KS orbital energy difference is quite far from the experimental value for this particular transition, it comes as no surprise that an expansion of the exact equation (15) around a single KS pole introduces a larger error than for states where this difference is smaller. The SMA performs clearly better, showing only deviations of a few tenths of a mHartree from the solution of the full matrix equation. This is most drastic for the $o\ ^1\Pi_u$ excited state, where the error of the SPA is strongly reduced by the SMA. As far as the deviations between the "full" solutions from the numerical code on one hand and the basis-set code on the other hand are concerned, there are two sources of error: the error introduced by the basis-set expansion and, in the case of the grid solution, the error resulting from the neglect of the continuum orbitals. As the differences are fairly small, being 6.1 mHartrees at the most (for the $A\ ^3\Sigma_u^+$ state), and as the errors caused by the use of basis set are of comparable magnitude, we conclude that the effect of the continuum contributions is of minor importance, at least for the lower excitation energies studied here. Finally, we note that the agreement of the calculated excitation energies with the

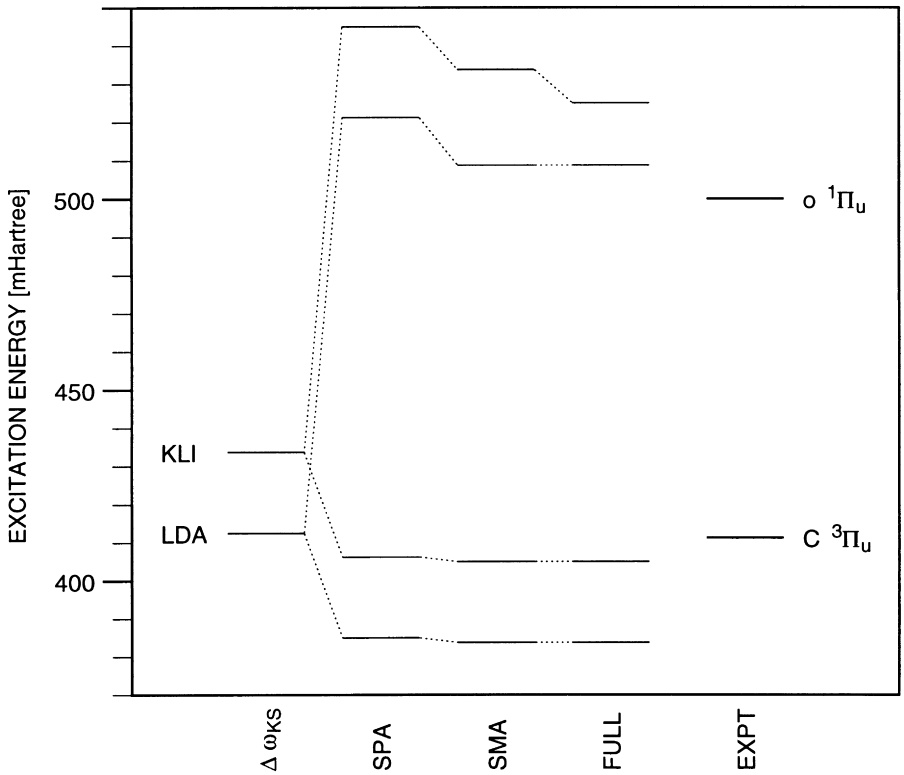

Fig. 1. The singlet–triplet splitting of the $2\sigma_u \rightarrow 1\pi_g$ KS transition in N_2 from the xcLDA and KLI calculations.

experimental values is very good for the lower states involving transitions to the $^1\Pi_g$ orbital. From Table 1 it is evident that the LDA-KS orbital-energy differences for these transitions are close to the (nearly exact) ones from the KLI potential. This indicates that a cancellation of the LDA self-interaction errors occurs, leading to the excellent results for the lower excitation energies. Values corresponding to transitions to the $4\sigma_g$ orbital, however, underestimate the experimental values considerably, reflecting the fact that the error cancellation for the KS orbital energy differences ceases to work so well.

In order to study the effect of the KS potential on the excitation energies, we have also performed calculations with the KLI and KLICS potential, presented in Tables 3 and 4, respectively. As before, the xc kernels were approximated by the ALDA. Hence the changes in the calculated excitation energies as compared to the results of Table 2 are solely due to the different KS potentials used. The columns headed "full" display solutions of Eq. (17) taking into account all 15 orbitals listed in Table 1. As far as the performance of the SPA and SMA is concerned, a picture similar to the LDA results is found: both approximations work very well, except that the SPA shows larger errors when the KS orbital-energy difference is further away from the experimental value, as is the case for the o $^1\Pi_u$ state. Comparison with the experimental values shows that the agreement with the calculated ones is very good. In contrast to the LDA results, this is also true for the higher excitations involving transitions to other than the $1\pi_g$ orbital. Generally, the calculated values are higher in energy than the ones from the LDA approach. This is primarily due to the larger KS orbital-energy differences and clearly visible in Fig. 1. There we have plotted the resulting excitation energies for the $2\sigma_u \rightarrow 1\pi_g$ transition in LDA and KLI approximation in order to visualize the effect of the various truncation approximations on the resulting excitation energies. Finally, the KLICS scheme leads to slightly larger orbital-energy differences and excitation energies than the

Table 5
Excitation energies for N_2 from various methods at $R = 2.0744$ a.u. The ALDA was employed for the xc kernels in the DFT calculations. Dev denotes the mean absolute deviation from the experimental values for all 12 states. All numbers in mHartrees

State	LDA[a]	KLI[b]	KLICS[c]	LB[d]	$\frac{\text{KLI} + \text{LB}}{2}$	MRCC-SD[e]	Expt[f]
$A\ ^3\Sigma_u^+$	296.7	312.8	312.9	267.9	290.4	277.8	284.5
$B\ ^3\Pi_g$	280.1	298.7	297.6	262.4	280.6	296.0	295.5
$W\ ^3\Delta_u$	327.6	343.2	343.8	305.8	324.5	328.1	326.3
$a\ ^1\Pi_g$	339.4	358.7	358.1	319.0	338.9	340.8	342.1
$B'\ ^3\Sigma_u^-$	355.8	370.9	371.9	337.4	354.2	362.5	355.4
$a'\ ^1\Sigma_u^-$	355.8	370.9	371.9	337.4	354.2	370.7	364.6
$w\ ^1\Delta_u$	377.6	392.0	393.4	360.9	376.5	387.4	377.4
$C\ ^3\Pi_u$	383.7	406.4	404.7	369.7	388.1	411.2	411.2
$E\ ^3\Sigma_g^+$	379.8	439.7	456.1	452.7	446.2	431.9	441.0
$a''\ ^1\Sigma_g^+$	385.3	458.1	476.3	–	–	448.3	448.3
$c\ ^1\Pi_u$	435.3	480.3	500.8	–	–	471.9	474.1
$o\ ^1\Pi_u$	509.8	526.2	525.9	–	–	504.0	500.9
Dev	20.0	12.4	17.1	(23.1)	(7.4)	4.0	

[a] Full matrix neglecting continuum states.
[b] Full matrix using all occupied and the lowest 9 unoccupied orbitals.
[c] Full matrix using all occupied and the lowest 9 unoccupied orbitals.
[d] From Ref. [36].
[e] From Ref. [43].
[f] From Ref. [43].

KLI approximation, thus shifting the calculated results further away from the experimental ones in most cases.

The excitation energies calculated using the three DFT approaches are compared in Table 5 and Fig. 2 with results from a multi-reference coupled cluster (MRCC) calculation from Ref. [43]. On an average, the KLI potential leads to the best results of the three DFT methods with a mean absolute deviation of 12.4 mHartrees from the experimental values. The use of the LDA potential gives a deviation of 20.0 mHartrees whereas the KLICS results lie in between, showing a deviation of 17.1 mHartrees. For comparison, we have also listed excitation energies given in Ref. [36], which were obtained from the model potential of van Leeuwen and Baerends [63] (LB). The corresponding results deviate by 23.1 mHartrees from the experimental spectrum. Clearly, the computationally much more expensive MRCC calculations lead to considerably better results with a deviation of 4.0 mHartrees. Furthermore, the quality of the LDA results depends very sensitively on the state under consideration: for the eight lowest excited states, the mean absolute deviation from the experimental values is only 8.6 mHartrees, whereas it is 43.0 mHartrees for the four higher states shown in Table 5 and Fig. 2. A similar picture is found for the KLICS results. Here, the mean absolute errors are 13.8 and 23.7 mHartrees for the eight lowest and four higher states, respectively. From the DFT methods, only the use of the KLI potential leads to results with comparable accuracy for all states. In this approximation, the errors are 13.3 mHartrees for the eight lowest and 10.7 mHartrees for the four higher excited states. While the excitation energies tend to be overestimated by the KLI and KLICS potentials, they tend to be underestimated by the LB potential. This is especially true for the lowest eight states, where the errors of both potentials are of opposite sign and are at the same time almost equal in magnitude. This is illustrated by column 6 of Table 5, where the arithmetic mean of the KLI and the LB energies are displayed. The values given in this column are close to the experimental spectrum (with a mean absolute deviation of 7.4 mHartrees). However, the KLI potential alone seems to give the best representation of the higher Rydberg states. Of course, the MRCC results show consistent accuracy for all states as well: For the eight lowest states, the error is 4.2 mHartrees, for the higher ones it is 3.6 mHartrees. Nevertheless, the

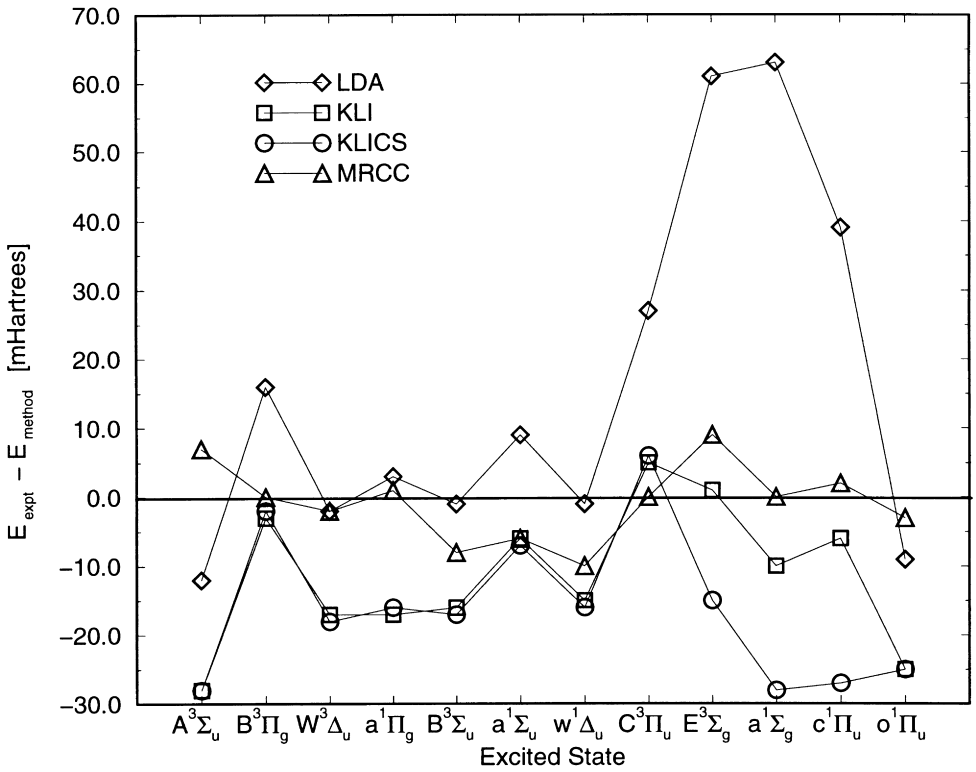

Fig. 2. Difference of experimental and calculated excitation energies of N_2 corresponding to Table 5. On the *x*-axis, the excited states are ordered according to their experimental excitation energy with the energy increasing from left to right in arbitrary units.

Table 6
Orbital energies for CO at $R = 2.1322$ a.u. from various DFT approaches

	xcLDA	KLI	KLICS
E_{TOT}	−112.4782	−112.7832	−113.2616
Occupied orbitals:			
1σ	−18.7186	−19.0959	−19.1349
2σ	−9.9072	−10.2983	−10.3406
3σ	−1.0753	−1.3280	−1.3607
4σ	−0.5216	−0.7599	−0.7920
1π	−0.4455	−0.6738	−0.7067
5σ	−0.3351	−0.5526	−0.5812
Unoccupied orbitals:			
2π	−0.0829	−0.2853	−0.3159
6σ	−0.0019	−0.1631	−0.1774
3π	> 0	−0.1208	−0.1304
7σ	> 0	−0.1203	−0.1292
8σ	> 0	−0.0772	−0.0845
1δ	> 0	−0.0771	−0.0836
4π	> 0	−0.0684	−0.0721
9σ	> 0	−0.0639	−0.0666
10σ	> 0	−0.0530	−0.0550

quality of the DFT results is astounding, considering the simplicity of the approach. Especially, the relatively small deviation of the eight lowest states obtained with the LDA potential is impressive. We note that a third-order many-body perturbation theory calculation gives an error of the same magnitude for these states [43].

A similar picture is found for CO. The orbital energies resulting from calculations using the LDA, KLI and KLICS potentials are shown in Table 6. As for N_2, the LDA potential decreases too rapidly in the valence region, leading to only two bound states and a value for ϵ_{HOMO} of −335 mHartrees. This is far above the experimentally observed first ionization potential of −515 mHartrees [64]. The KLI value of −553 mHartrees is much closer, whereas adding the CS correlation potential moves the orbital energy further from the exact one, yielding −581 mHartrees. Again, on average, the results from using the KLI potential are closest to the experimental values.

In Table 7 the excitation energies resulting from an

Table 7
Excitation energies for CO from an xcLDA-calculation at $R = 2.1322$ a.u. The LDA was employed for V_{xc} and the ALDA for the xc kernels. $\Delta\omega_{KS}$ denotes the KS orbital energy difference. All numbers in mHartrees

State		$\Delta\omega_{KS}$	SPA	SMA	Full[a]	Exp[b]
A $^1\Pi$	$5\sigma \rightarrow 2\pi$	252.3	326.8	318.2	310.2	312.7
a $^3\Pi$			223.8	222.0	221.4	232.3
B $^1\Sigma^+$	$5\sigma \rightarrow 6\sigma$	333.2	338.9	338.6	338.0	396.2
b $^3\Sigma^+$			331.5	331.5	331.6	382.2
I $^1\Sigma^-$	$1\pi \rightarrow 2\pi$	362.6	362.6	362.6	362.6	363.1
e $^3\Sigma^-$			362.6	362.6	362.6	363.1
a′ $^3\Sigma^+$			318.1	315.0	314.9	312.7
D $^1\Delta$			381.2	380.7	380.7	375.9
d $^3\Delta$			340.4	339.6	339.6	344.0
c $^3\Pi$	$4\sigma \rightarrow 2\pi$	438.8	420.4	420.0	420.2	424.5
E $^1\Pi$	$1\pi \rightarrow 6\sigma$	443.6	443.5	443.5	443.5	423.7

[a] Neglecting continuum states.
[b] From Ref. [65].

LDA calculation are shown. The SPA and SMA lead to results close to the ones from the full solution of the matrix Eq. (17) taking into account all nine bound orbitals. Generally, the SMA shows the smaller error. Again, the largest deviations arise for states such as A $^1\Pi$ where the corresponding KS orbital energy difference is far away from the exact excitation energy. On the whole, it is apparent that excitation energies involving transitions to the 2π KS orbital are reproduced very well, whereas transitions to the 6σ orbital show a larger error. A glance at the orbital energies given in Table 4 indicates that while the KS orbital energy difference is of comparable magnitude for the transitions to the 2π KS orbital in all approximations, it is quite different for the transitions to the 6σ orbital. For the latter, the LDA orbital-differences are substantially smaller than the ones calculated from the more accurate KLI potential, leading to excitation energies which are too low.

Table 8
Excitation energies for CO from a KLI-calculation at $R = 2.1322$ a.u. The exact exchange was employed for V_{xc} in KLI-approximation and the ALDA for the xc kernels. $\Delta\omega_{KS}$ denotes the KS orbital energy difference. All numbers in mHartrees

State		$\Delta\omega_{KS}$	SPA	SMA	Full[a]	Exp[b]
A $^1\Pi$	$5\sigma \rightarrow 2\pi$	267.4	345.8	336.8	327.2	312.7
a $^3\Pi$			237.0	235.0	234.2	232.3
I $^1\Sigma^-$	$1\pi \rightarrow 2\pi$	388.6	388.6	388.6	388.6	363.1
e $^3\Sigma^-$			388.6	388.6	388.6	363.1
a′ $^3\Sigma^+$			346.7	344.2	343.4	312.7
D $^1\Delta$			405.6	405.2	405.2	375.9
d $^3\Delta$			367.6	367.0	366.9	344.0
B $^1\Sigma^+$	$5\sigma \rightarrow 6\sigma$	389.6	409.4	408.9	402.4	396.2
b $^3\Sigma^+$			383.8	383.7	383.5	382.2
E $^1\Pi$	$5\sigma \rightarrow 3\pi$	431.8	430.8	430.8	431.1	423.7
c $^3\Pi$			429.2	429.2	429.1	424.5
C $^1\Sigma^+$	$5\sigma \rightarrow 7\sigma$	432.3	437.7	437.7	436.4	418.9
j $^3\Sigma^+$			427.0	427.0	427.0	415.3
F $^1\Sigma^+$	$5\sigma \rightarrow 8\sigma$	475.4	477.8	477.8	475.5	455.7

[a] Using all occupied and the lowest 9 unoccupied orbitals.
[b] From Ref. [65].

Table 9
Excitation energies for CO from a KLICS-calculation at $R = 2.1322$ a.u. The CS approximation for correlation added to the exact exchange was employed for V_{xc} in KLI-approximation and the ALDA for the xc kernels. $\Delta\omega_{KS}$ denotes the KS orbital energy difference. All numbers in mHartrees

State		$\Delta\omega_{KS}$	SPA	SMA	Full[a]	Exp[b]
A $^1\Pi$	$5\sigma \rightarrow 2\pi$	265.2	345.0	335.7	326.2	312.7
a $^3\Pi$			234.3	232.3	231.4	232.3
I $^1\Sigma^-$	$1\pi \rightarrow 2\pi$	390.8	390.8	390.8	390.8	363.1
e $^3\Sigma^-$			390.8	390.8	390.8	363.1
a′ $^3\Sigma^+$			348.2	345.6	344.8	312.7
D $^1\Delta$			408.1	407.7	407.7	375.9
d $^3\Delta$			369.5	368.8	368.7	344.0
B $^1\Sigma^+$	$5\sigma \rightarrow 6\sigma$	403.8	425.3	424.8	417.5	396.2
b $^3\Sigma^+$			397.5	397.4	397.2	382.2
E $^1\Pi$	$5\sigma \rightarrow 3\pi$	450.7	449.6	449.6	449.7	423.7
c $^3\Pi$			447.9	447.9	447.5	424.5
C $^1\Sigma^+$	$5\sigma \rightarrow 7\sigma$	451.9	459.3	459.2	457.2	418.9
j $^3\Sigma^+$			445.7	445.6	445.6	415.3
F $^1\Sigma^+$	$5\sigma \rightarrow 8\sigma$	496.7	499.8	499.8	497.0	455.7

[a] Using all occupied and the lowest 9 unoccupied orbitals.
[b] From Ref. [65].

Consequently, this should not be the case, if the KLI or KLICS potentials are used instead of the LDA. This is clearly visible from Tables 8 and 9. Most notably, the energetic ordering of the orbital-energy differences corresponding to the $1\pi \rightarrow 2\pi$ and the $5\sigma \rightarrow 6\sigma$ transition is reversed compared to the LDA calculation. Furthermore, in KLI and KLICS calculations the c $^3\Pi$ and E $^1\Pi$ excited states are assigned to correspond to a $5\sigma \rightarrow 3\pi$ KS transition, whereas they arise from the $4\sigma \rightarrow 2\pi$ and $1\pi \rightarrow 6\sigma$ transitions, respectively, if the LDA potential is used. Compared to the LDA, the quality of the results for these higher lying excited states is increased

Table 10
Lower excitation energies for CO from various methods at $R = 2.1322$ a.u. The ALDA was employed for the xc kernels in the DFT calculations. Dev denotes the mean absolute deviation for all 11 states. All numbers in mHartrees

State	LDA[a]	KLI[b]	KLICS[c]	LB[d]	MR-CCSD[e]	SOPPA[f]	Expt[g]
a $^3\Pi$	221.4	234.2	231.4	205.1	232.3	219.4	232.3
A $^1\Pi$	310.2	327.2	326.2	293.3	321.2	310.9	312.7
a$'$ $^3\Sigma^+$	314.9	343.4	344.8	307.2	308.3	293.6	312.7
d $^3\Delta$	339.6	366.9	368.7	337.0	343.2	328.5	344.0
I $^1\Sigma^-$	362.6	388.6	390.8	–	371.5	356.5	363.1
e $^3\Sigma^-$	362.6	388.6	390.8	362.3	366.4	354.6	363.1
D $^1\Delta$	380.7	405.2	407.7	–	377.0	366.0	375.9
dev	3.7	21.5	22.6	(12.0)	3.8	10.6	

[a] Full matrix neglecting continuum states.
[b] Full matrix using all occupied and the lowest 9 unoccupied orbitals.
[c] Full matrix using all occupied and the lowest 9 unoccupied orbitals.
[d] From Ref. [36].
[e] From Ref. [66].
[f] From Ref. [66].
[g] From Ref. [65].

significantly if the KLI potential is used. However, the KLICS potential overestimates the resulting excitation energies considerably, especially for the higher lying states. For both approaches, the SPA and SMA give results in close agreement with the ones from the full solution of Eq. (15), except for the $5\sigma \rightarrow 2\pi$ singlet transition where the KS orbital difference is far from the experimental value.

In Table 10 and Fig. 3 we compare our results for the seven lowest excited states of CO with those obtained from the MRCC method and the second order polarization propagator approach (SOPPA) [66]. Here, the LDA leads to the best results with an average mean absolute deviation from the experimental values of 3.7 mHartrees, whereas the MRCC approach leads to an error of 3.8 mHartrees. For these lower states, both the KLI and KLICS again overestimate the excitation energies with a deviation of 21.5 and 22.6 mHartrees, respectively. The LB-potential underestimates the transition energies, but with a mean deviation of only 12 mHartrees for the states shown.

However, for the higher states a different picture is found, as may be seen from Table 11 and Fig. 3. For these states, the KLI results are best with a mean absolute deviation of 4.9 mHartrees, which is better than the MRCC results, which do show an error of 5.4 mHartrees. The LDA performs poorly leading to an average error of 33.2 mHartrees.

If all 11 states are taken into account, the conventional quantum chemistry methods are superior on average, with a mean absolute deviation well below 10 mHartrees for the eleven states listed. The DFT approaches show a larger error, worst among them the KLICS results with 22.2 mHartrees. The LDA and KLI potentials lead to an almost equivalent average deviation of 14.4 and 15.4 mHartrees, respectively.

5. Summary and conclusion

The main purpose of this work was to study the performance of various approximations involved in the calculation of molecular excitation energies from time-dependent DFT. Starting from the (unphysical) KS spectrum, we obtained corrections towards the physical excitation energies for the N_2 and the CO molecule.

First of all, the calculation of response properties, which in principle involves an infinite number KS orbitals, requires a truncation of the problem in one way or another. For the excitation energies studied in this work, the single-pole approximation (SPA), which, in a nondegenerate situation, only requires one occupied (initial) and one virtual (final) KS orbital, already gives results which are quite close to more refined approximations ("full") using more configurations. Since the SPA

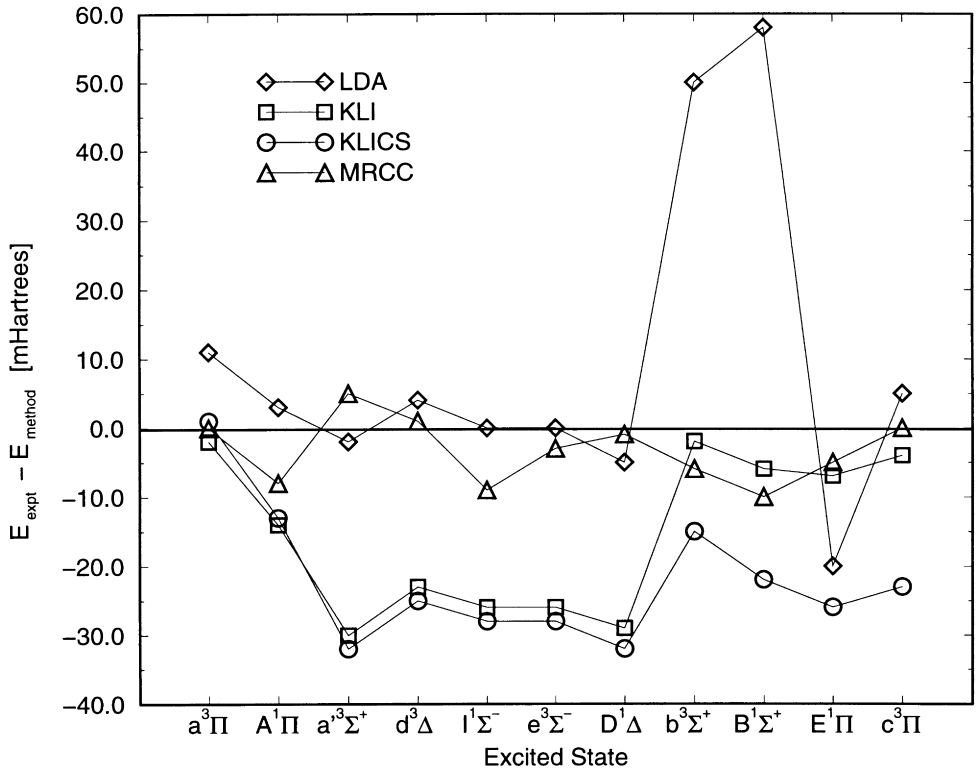

Fig. 3. Difference of experimental and calculated excitation energies of CO corresponding to Tables 10 and 11. On the *x*-axis, the excited states are ordered according to their experimental excitation energy with the energy increasing from left to right in arbitrary units.

allows a simple assignment of excitation energies, it can serve as a first orientation in practical calculations.

Next, we have calculated excitation energies using different exchange-correlation potentials. In this context, the LDA was tested against (self-interaction free) orbital approximations. Our calculations show, that in order to obtain spectra from DFT which are close to experiment, the underlying KS eigenvalue differences have to be well represented.

In agreement with the results of Casida et al. [36], it was found that the LDA potential yields excellent results for lower excitation energies of molecules. For these excitations, the relatively large self-interaction errors, which are present in the LDA-orbital energies, cancel to a large extent. This finally leads to a fairly good representation of the true KS eigenvalue differences.

However, this cancellation of errors ceases to work for excitations to higher lying states. There, the correct asymptotic behaviour of the xc potential is essential. In this regime, orbital functionals based on exact exchange in the approximation of Krieger, Li and Iafrate (KLI) performed very well. However, these potentials show a tendency to overestimate the molecular excitation energies. The inclusion of correlation contributions in the form of Colle and Salvetti (CS) consistently worsened the results, indicating that the CS correlation potential needs improvement for the calculation of molecular properties. This overestimation is most pronounced for lower excitation energies, which in turn are very well represented by the LDA.

On the whole, the quality of the results obtained with the DFT scheme for excitation energies is very encouraging. Improvements are however necessary for the correlation potential. In our opinion, orbital functionals offer a viable route in this direction.

Table 11
Higher excitation energies for CO from various methods at $R = 2.1322$ a.u. The ALDA was employed for the xc kernels in the DFT calculations. Dev denotes the mean absolute deviation for all 11 states. All numbers in mHartrees

State	LDA[a]	KLI[b]	KLICS[c]	MR-CCSD[d]	SOPPA[e]	Expt[f]
b $^3\Sigma^+$	331.6	383.5	397.2	388.1	381.1	382.2
B $^1\Sigma^+$	338.0	402.4	417.5	405.7	398.0	396.2
E $^1\Pi$	443.5	431.1	449.7	429.2	422.2	423.7
c $^3\Pi$	420.2	429.1	447.5	425.2	418.6	424.5
dev	33.2	4.9	21.3	5.4	2.6	

[a] Full matrix neglecting continuum states.
[b] Full matrix using all occupied and the lowest 9 unoccupied orbitals.
[c] Full matrix using all occupied and the lowest 9 unoccupied orbitals.
[d] From Ref. [66].
[e] From Ref. [66].
[f] From Ref. [65].

Acknowledgements

We thank D. Sundholm and P. Pyykkö for providing us with their two-dimensional Xα code for molecules [62]. This work was supported by the Deutsche Forschungsgemeinschaft.

References

[1] P. Hohenberg, W. Kohn, Phys. Rev. B 136 (1964) 864.
[2] W. Kohn, L.J. Sham, Phys. Rev. A 140 (1965) 1133.
[3] R.G. Parr, W. Yang, Density-Functional Theory of Atoms and Molecules, Oxford University Press, New York, 1989.
[4] R.M. Dreizler, E.K.U. Gross, Density Functional Theory, an Approach to the Quantum Many-Body Problem, Springer, Berlin, 1990.
[5] E.K.U. Gross, R.M. Dreizler (Eds.), Density Functional Theory NATO ASI Series B, 337, Plenum Press, New York, 1995.
[6] T. Grabo, E.K.U. Gross, Chem. Phys. Lett. 240 (141) 1995 erratum: 241 (1995) 635.
[7] O. Gunnarsson, B.I. Lundqvist, Phys. Rev. B 13 (1976) 4274.
[8] T. Ziegler, A. Rauk, E.J. Baerends, Theor. Chim. Acta 43 (1977) 261.
[9] U. von Barth, Phys. Rev. A 20 (1979) 1693.
[10] A. Theophilou, J. Phys. C 12 (1979) 5419.
[11] N. Hadjisavvas, A. Theophilou, Phys. Rev. A 32 (1985) 720.
[12] W. Kohn, Phys. Rev. A 34 (1986) 5419.
[13] E.K.U. Gross, L.N. Oliveira, W. Kohn, Phys. Rev. A 37 (1988) 2805.
[14] E.K.U. Gross, L.N. Oliveira, W. Kohn, Phys. Rev. A 37 (1988) 2809.
[15] L.N. Oliveira, E.K.U. Gross, W. Kohn, Phys. Rev. A 37 (1988) 2821.
[16] A. Nagy, Phys. Rev. A 42 (1990) 4388.
[17] A. Nagy, J. Phys. B 24 (1991) 4691.
[18] A. Nagy, Phys. Rev. A 49 (1994) 3074.
[19] A. Nagy, Int. J. Quantum Chem. 56 (1995) 225.
[20] A. Nagy, Int. J. Quantum Chem. Symp. 29 (1995) 297.
[21] A. Nagy, J. Phys. B 29 (1996) 389.
[22] A. Nagy, Adv. Quant. Chem. 29 (1997) 159.
[23] I. Andrejkovics, A. Nagy, Chem. Phys. Lett. 296 (1998) 489.
[24] M. Petersilka, Diplomarbeit, Universität Würzburg, 1993.
[25] M. Petersilka, E.K.U. Gross, Satellite Symposium of the 8th International Congress of Quantum Chemistry, Cracow, Poland, Book of Abstracts, 1994.
[26] E.K.U. Gross, 209th American Chemical Symposium of the Eighth International Congress of Quantum Chemistry (1995) 112.
[27] M. Petersilka, U.J. Gossmann, E.K.U. Gross, Phys. Rev. Lett. 76 (1996) 1212.
[28] M. Petersilka, E.K.U. Gross, Int. J. Quantum Chem. 60 (1996) 181.
[29] E. Runge, E.K.U. Gross, Phys. Rev. Lett. 52 (1984) 997.
[30] M. Petersilka, U. Gossmann, E.K.U. Gross, in: G. Vignale, J.F. Dobson, M.P. Das (Eds.), Electronic Density Functional Theory: Recent Progress and New Directions, Plenum Press, New York, 1988, p. 177.
[31] S.J.A. van Gisbergen, F. Kootstra, P.R.T. Schipper, O.V. Gritsenko, J.G. Snijders, E.J. Baerends, Phys. Rev. A 57 (1998) 2556.
[32] M. Petersilka, PhD thesis, Universität Würzburg, 1998.
[33] Ch. Jamorski, M.E. Casida, D.R. Salahub, J. Chem. Phys. 104 (1996) 5134.
[34] R. Bauernschmitt, R. Ahlrichs, Chem. Phys. Lett. 256 (1996) 454.
[35] R. Bauernschmitt, M. Hauser, O. Treutler, R. Ahlrichs, Chem. Phys. Lett. 264 (1997) 573.
[36] M.E. Casida, C. Jamorski, K.C. Casida, D.R. Salahub, J. Chem. Phys. 108 (1998) 4439.
[37] S.J.A. van Gisbergen, PhD thesis, Vrije Universiteit, Amsterdam, 1998.
[38] M.E. Casida, K.C. Casida, D.R. Salahub, Int. J. Quantum Chem. 70 (1998) 933.
[39] A. Rubio, J.A. Alonso, X. Blase, L.C. Balbas, S.G. Louie, Phys. Rev. Lett. 77 (1996) 247.
[40] J.M. Pacheco, J.L. Martins, J. Chem. Phys. 106 (1997) 6039.
[41] I. Vasiliev, S. Ögüt, J.R. Chelikowsky, Phys. Rev. Lett. 82 (1999) 1919.
[42] E.K.U. Gross, E. Runge, O. Heinonen, Many-Particle Theory, Adam Hilger, IOP Publishing, Bristol, 1991.
[43] S.B. Ben-Shlomo, U. Kaldor, J. Chem. Phys. 92 (1990) 3680.
[44] S.H. Vosko, L. Wilk, M. Nusair, Can. J. Phys. 58 (1980) 1200.
[45] J.B. Krieger, Y. Li, G.J. Iafrate, Phys. Lett. A 146 (1990) 256.
[46] J.B. Krieger, Y. Li, G.J. Iafrate, Int. J. Quantum Chem. 41 (1992) 489.
[47] J.B. Krieger, Y. Li, G.J. Iafrate, Phys. Rev. A 46 (1992) 5453.
[48] J.B. Krieger, Y. Li, G.J. Iafrate, Chem. Phys. Lett. 191 (1992) 38.

[49] J.B. Krieger, Y. Li, G.J. Iafrate, Phys. Rev. A 45 (1992) 101.
[50] Y. Li, J.B. Krieger, G.J. Iafrate, Phys. Rev. A 47 (1993) 165.
[51] J.B. Krieger, Y. Li, G.J. Iafrate, in: E.K.U. Gross, R.M. Dreizler (Eds.), Density Functional Theory, NATO ASI Series B, 337, Plenum, New York, 1995, p. 191.
[52] R. Colle, D. Salvetti, Theor. Chim. Acta 37 (1975) 329.
[53] R. Colle, D. Salvetti, Theor. Chim. Acta 53 (1979) 55.
[54] T. Grabo, T. Kreibich, E.K.U. Gross, Mol. Engng 7 (1997) 27.
[55] T. Kreibich, S. Kurth, T. Grabo, E.K.U. Gross, Adv. Quantum Chem. 33 (1999) 31.
[56] T. Grabo, T. Kreibich, S. Kurth, E.K.U. Gross, in: V.I. Anisimov (Ed.), Strong Coulomb Correlations in Electronic Structure Calculations, Gordon and Breach, London, 1999, pp. 203–311.
[57] T. Grabo, E.K.U. Gross, Int. J. Quantum Chem. 64 (1997) 95.
[58] E.K.U. Gross, J.F. Dobson, M. Petersilka, in: R.F. Nalewajski (Ed.), Density Funcional Theory II, Topics in Current Chemistry, 181, Springer, Berlin, 1996, p. 81.
[59] L. Laaksonen, P. Pyykkö, D. Sundholm, Int. J. Quantum Chem. 23 (1983) 309.
[60] L. Laaksonen, P. Pyykkö, D. Sundholm, Int. J. Quantum Chem. 23 (1983) 319.
[61] L. Laaksonen, D. Sundholm, P. Pyykkö, Int. J. Quantum Chem. 28 (1985) 601.
[62] L. Laaksonen, P. Pyykkö, D. Sundholm, Comp. Phys. Rep. 4 (1986) 313.
[63] R. van Leeuwen, E.J. Baerends, Phys. Rev. A 49 (1994) 2421.
[64] K.P. Huber, G. Herzberg, Molecular Spectra and Molecular Structure: IV. Constants of Diatomic Molecules, Van Nostrand Reinhold, New York, 1979.
[65] E.S. Nielsen, P. Jørgensen, J. Oddershede, J. Chem. Phys. 73 (1980) 6238.
[66] J. Geertsen, M. Rittby, J. Bartlett, Chem. Phys. Lett. 164 (1989) 57.